REPORT DOCUMENTATION PAGE

AFRL-SR-AR-TR-02-

0451

Public reporting burden for this collection of information is estimated to average 1 hour per response, including the time for reviewing instructions, search the collection of information. Send comments regarding this burden estimate or any other aspect of this collection of information, including suggest Operations and Reports, 1215 Jefferson Davis Highway, Suite 1204, Arlington, VA 22202-4302, and to the Office of Management and Budget, Paperwo

1. AGENCY USE ONLY *(Leave blank)*	2. REPORT DATE	3. REPORT TYPE AND DATES COVERED
		01 May 99 - 28 Feb 02

4. TITLE AND SUBTITLE
MATHEMATICAL MODELING, SIMULATION, AND CONTROL OF PHYSICAL PROCESSES

5. FUNDING NUMBERS
F49620-99-1-0261

6. AUTHOR(S)
THOMAS SVOBODNY

7. PERFORMING ORGANIZATION NAME(S) AND ADDRESS(ES)
DEPARTMENT OF MATHEMATICS AND STATISTICS
DEPARTMENT OF PHYSICS
WRIGHT STATE UNIVERSITY
DAYTON, OH 45435

8. PERFORMING ORGANIZATION REPORT NUMBER

9. SPONSORING/MONITORING AGENCY NAME(S) AND ADDRESS(ES)
AFOSR/NM
4015 Wilson Blvd, Room 713
Arlington, VA 22203-1954

10. SPONSORING/MONITORING AGENCY REPORT NUMBER
F49620-99-1-0261

11. SUPPLEMENTARY NOTES

12a. DISTRIBUTION AVAILABILITY STATEMENT
APPROVED FOR PUBLIC RELEASE, DISTRIBUTION UNLIMITED

12b. DISTRIBUTION CODE

13. ABSTRACT *(Maximum 200 words)*

Concerning the ablation plume phenomenon, a computational model for the interaction of laser energy with solid matter was developed, as well as analytical and computational models for the lume hydrodynamics, including the chemical reactions. A first task was to understand which variables are the most important. There are approximately 20 input variables that can be varied during the process. Some of these are fied parameters, other depend on time, while others, such as electromagnetics, are (time-varying) fields. Contrasted with the many input variables are the desired outcomes from the film. Naturally, there is not time for experiments that vary all of the inputs and to measure the effect on these outcomes as the dimensional complexity is overwhelming. We needed to reduce the experimental effort, via straightforward polynomial regression experimental design and adaptive learning data mining response surface methods. The interaction of laser energy with a solic material takes many different forms depending on the power input and the material properties. That is, thermal conducton is the main methods of energy transport. The justification is that energy transferred is spread out over a vibrationally long time period.

20030115 090

14. SUBJECT TERMS	15. NUMBER OF PAGES
	27
	16. PRICE CODE

17. SECURITY CLASSIFICATION OF REPORT	18. SECURITY CLASSIFICATION OF THIS PAGE	19. SECURITY CLASSIFICATION OF ABSTRACT	20. LIMITATION OF ABSTRACT

Standard Form 298 (Rev. 2-89) (EG)
Prescribed by ANSI Std. 239.18
Designed using Perform Pro, WHS/DIOR, Oct 94

MATHEMATICAL MODELING, SIMULATION, AND CONTROL OF PHYSICAL PROCESSES

AFOSR F49620-99-1-0261

FINAL TECHNICAL REPORT

Thomas P. Svobodny

Department of Mathematics and Statistics
Department of Physics

Wright State University
Dayton, OH 45435

thomas.svobodny@wright.edu
http://www.math.wright.edu/ms/appliedmath/svobodny.html

Objectives

The main goal of this program has been to support the immediate needs of the Air Force as well as being relevant to long range Air Force *defense-after-next* plans. The program includes basic research that is expected to serve a role in the long-range goals of the Air Force. The focus of this research has been to support the scientists at Air Force Research Laboratory at Wright-Patterson Air Force Base involved in advanced technological materials processing. The foremost goal was to model the pulsed-laser ablation plume dynamics. This is the necessary first step towards a process modeling and control of the Pulsed-Laser-Deposition (PLD) process of materials such as the the high-temperature superconductor Yttrium_1 Barium_2 Copper_3 Oxygen (YBCO). The AFRL has a multi-directorate team led by J. Maguire and R. Biggers which is focussed on making large specimens of YBCO. However, besides YBCO, there are other related compounds: CuO, CeO_2, ZrO_2, Y_2O_3, and YSZ. Some of these compounds are needed in the processing of YBCO, while others are simplified material models to aid in understanding YBCO. Films made by PLD include superconductors, ferroelectric ceramic films, transparent conducting films, lubricant films, and semi-conductors. Film quality can be extremely high; however, consistency in results still falls far short of what is needed before turning the task over to a manufacturing team. The main factor hampering this transfer has been a lack of model-based control. A long-term goal is the

DISTRIBUTION STATEMENT A
Approved for Public Release
Distribution Unlimited

a matrix which may or may not itself be magnetic. Most of the quantitative work on the magnetocaloric effect has not been very accurate. This is because the interactions of the spin thermodynamic system with the underlying elastic vibrations has not been taken into account. The full interaction is very difficult, since, even under the assumption of linear elasticity and linearized magnetism, where the excitations are phonons and magnons, the magneto-elastic interaction is inescapably non-linear. An objective of this research program has been to study models, where the magnon and phonon branches of the spectrum combine to give a new type of excitation that is used for the quantum statistics. What is very interesting is that these *quasi-phonons* can have a spectral branch that disappears near a phase transition.

Accomplishments/Findings

Concerning the ablation plume phenomenon, a computational model for the interaction of laser energy with solid matter was developed, as well as analytical and computational models for the plume hydrodynamics, including the chemical reactions. A first task was to understand which variables are the most important. There are approximately 20 input variables that can be varied during the process. Some of these are fixed parameters, other depend on time, while others, such as electromagnetics, are (time-varying) fields. Contrasted with the many input variables are the desired outcomes for the film. Naturally, there is not time for experiments that vary all of the inputs and to measure the effect on these outcomes as the dimensional complexity is overwhelming. We needed to reduce the experimental effort, via straightforward polynomial regression experimental design and adaptive learning data mining, response surface methods, The interaction of laser energy with a solid material takes many different forms depending on the power input and the material properties. We have modeled this using a phase change approach to the thermal development. That is, thermal conduction is the main method of energy transport. The justification is that the energy transferred is spread out over a vibrationally long time period. The important thing is to know the composition (in multi-component phase space) of the plasma cloud as it begins its expansion. There is an important role played by the hydrodynamics (shock heating, mixing) in the stoichiometry and equilibrium flux onto the substrate. A focus of the present effort was on figuring out exactly what the time-of-flight measurement is telling us about the physics in the plume and energy flow thereinto, since it is the major output, and is currently used as a manual control. There are interesting features of the time-of-flight signature, such as double peaking, that are presently the object of intense debate. We have identified several sources for these phenomena, including reflected shocks, shock-

complete modeling and theory necessary for an eventual automatic control of this process. Towards that long term goal, a necessary first step and an immediate goal of the research program has been the physical and mathematical modeling of the reacting plume itself. There are three main physical subprocesses occuring during the PLD process. These are the 1) Ablation Process, where photons are absorbed by the target, resulting in heating and chemical disassembly, and release of vapor, 2) Plume Dynamics, where a plasma cloud expands and suffers self-collisions and collisions with the ambient gas, 3) Deposition and Growth. Since the output of each sub-process supplies input for the next process, there has been some expectation that the modeling should follow this sequence; however, we have found that, although there is some separation of time scales from one sub-process to the next, there is also considerable feedback and mutual exchange of energy. The science involved is at the extremes of energy and stability, governed by highly nonlinear processes, mainly due to the interaction of disparate physical scales in the same problem. The plume is very dynamic (supersonic, high-temperature, shocks, etc.) especially in the presence of a reacting background gas. (This is the case for deposition of YBCO, which requires an oxygen ambient). R. Biggers' lab has been running depositions for several years, and have accumulated much data concerning the plume: spectroscopic, time-of-flight, spatial distribution, etc. At the same time, post-processing measurements have been made of the resulting film (material and electromagnetic). A typical data file contains over 80 different entries for each sample. An objective was to study this data and make recommendations whenever necessary and look for ways to use the information in model building.

If the pulsed laser deposition process is ever to manufacture films that are needed by the Air Force (besides many other material systems of interest to AF and studied at AFRL, YBCO coated-conductors are envisioned for use in generators, especially in pulsed-power weapons and on aircraft, as well as in more advanced propulsion systems), the process will need to automatized. Automatic feedback control is a necessary part of this process.By-products of the same research program will be better material quality, more efficient use of facilities, and better system throughput, given that science and mathematical based processing control is easily adapted to the evolution of materials science and needs of the Air Force.

Another area of research that is of relevance to the Air Force and to the aerospace industry is modeling of magnetoelasticity, and more particularly, the magnetocaloric effect in magnetic and superconducting materials, taking into account magneto-elastic interactions. The magnetocaloric effect has been used at low temperatures in adiabatic demagnetization, but recently has been in the news as a possible method for refrigeration. A prototype of a refrigerator using the magnetocaloric effect has been built at the Astronautics Corporation. The materials used in these magnets are superparamagnetic nanoclusters: that is, they consist of magnetic nano-sized particles imbedded in

induced vorticity, charge separation and chemical species separation. There are reports from both experiment and simulation that show exagerated forward-direction to the plume. We have an analytic model to explain this. We have also been using simplified material systems (Cu, CuO, CeO) as tests of the basic model. Based on numerical ablation models, the number density of an ablated plume ranges from 10^{16} cm^{-3} to above 10^{20} cm^{-3}, depending on the energy input. With the energies used in film deposition in a background gas, one sees the latter range. Total particle energies in the nascent plume are typically in the range 4-17 eV. The translational energy is thermalized after only a few collisions per particle; we estimate a Knudsen number on the order of $10^{-4} - 10^{-2}$ in the flow domain behind the shock front – a mean free path is estimated at ≤ 0.1 mm. All the same, the particles evaporating or being ejected from the target will have a non-equilibrium distribution that will relax to a Maxwell-Boltzmann distribution after several (3-10) collisions. For ablation, or beam evaporation from a hot chamber, this takes place in a one-dimensional region nominally < 1 mm thick. For this reason, we treat this region here as an infinitesimal front much like a stationary shock. For given material parameters and laser beam energy, this and various other simulations and calculations supplies us with the values of hydrodynamic variables at the "outer" edge of the Knudsen layer, which is the inlet region for large-scale numerical computations. In very low pressure conditions the plume expansion can be described by a adiabatic expansion into vacuum. For expansion into a higher pressure ambient, there are two competing models for one dimensional plume expansion. The *blast wave model* describes the self-similar radial expansion when energy is deposited at a point at $t = 0$. The *normal shock model* describes one-dimensional motion peaked in a particular direction. Following closely on experiments, special solutions can be constructed each valid on scales widely separated from others. Computations also show this difference. However, in some situations the plume dynamics cannot be described by a one-dimensional model. The plume dynamics in the presence of a temperature gradient is one such example. Particularly in situations when the plume is seen to be extremely forwarded-directed. In experiments where substrate heat was isolated as a control, the plume showed an increase in size and emission intensity that was similar to the effect of increasing laser beam energy. However, in a vacuum, the heater produced no discernible change to the plume. Thus, the effect was due to molecular kinetics and not to radiative heat transfer. Moreover, this has been reproduced in our numerical computations, and has been explained via an analytical model. Two dimensional calculations of the complete multi-component reacting continuum fluid were carried out under a wide range of operating variables, including oxidation reactions. The main features of the plume shape in the presence of substrate heating, however, can be demonstrated with a one-component fluid. The difference between the computed plumes without substrate heating differ dramatically from the computed plumes in the presence of a temperature gradient, and corresponds to the difference that one sees in actuality. The development of vorticity is clearly indicated, as well as the one-dimensional jet-like flow. A compre-

hensive collection of simulation results, including animations, can be found on the web site of the PI listed above.

The excimer-type laser pulse lasts between tens of femtoseconds up to hundreds of nanoseconds. During this time, which can be long relative to the times characteristic of the basic interaction, the target material can become multi-phased as the solid melts and is ablated, either evaporatively or explosively. Furthermore, there is sometimes charge separation as a plasma cloud forms. Thus, there are several competing pathways for the light energy to be converted to other forms. On the shortest time scales, that of the optical excitation of electrons in a metal or of excitation of quasi-particles in a dielectric, one must take into account the disparate relaxation times of the electron system and the lattice-vibrational system of the solid. Thus, we consider two temperatures, T_e, the temperature of the electrons, and T_i, the temperature of the ions in the lattice. The interaction between these thermodynamic systems can be modeled via diffusion equations with a weak coupling between them:

$$C_e(T_e)\frac{\partial T_e}{\partial t} = \frac{\partial}{\partial z}(\frac{T_e}{T_i}k_e\frac{\partial T_e}{\partial z}) - B(T_e - T_i) + Q$$
$$C_i\frac{\partial T_i}{\partial t} = \frac{\partial}{\partial z}(k_i(T_i)\frac{\partial T_i}{\partial z}) + B(T_e - T_i),$$

where Q, the source term, is the laser power absorbed (in this example by electrons, bound or in conducting band), and z is the coordinate normal to the surface. It is reasonable to assume that the process is one-dimensional on the fast time scales where this model is valid. At later stages (on longer time-scales), the situation may be higher dimensional, but by that point the two thermodynamic systems can be considered to have achieved equilibrium with one another. Higher dimensional models are only really necessary for long pulsed systems or continuous (CW) laser work. The correct scaling depends on the the power absorption; for high power absorption ($\sim$GW cm^{-2}), the two temperature model is necessary in order to model the ablation, but for moderate intensities, where power is delivered over tens of nanoseconds, a single-temperature multi-phase thermal model may be sufficient. The material properties, like the optical properties, depend generally on the temperature and may be discontinuous at a phase boundary, so that we have the pair of equations,

$$c_s(T)\rho_s\frac{\partial}{\partial t}T_s = \frac{\partial}{\partial z}k_s(T)\frac{\partial T_s}{\partial z} + Q_s \quad (1)$$
$$c_l(T)\rho_l\frac{\partial}{\partial t}T_l = \frac{\partial}{\partial z}k_l(T)\frac{\partial T_l}{\partial z} + Q_l, \quad (2)$$

where the subscripts s and l refer to the solid and liquid regions, respectively. These equations are supplemented by the boundary condition,

$$T_s \to T_0, \quad z \to \infty, \quad (3)$$

where T_0 is the controlled heat of the workpiece or target, as well as conditions at the phase interfaces, $z = a_{sl}(t)$, and $z = a_{lv}(t)$. At the solid/liquid interface, conservation of energy requires

$$k_s \frac{\partial T_s}{\partial z} - k_l \frac{\partial T_l}{\partial z} = \rho_s L_m \frac{d}{dt} a_{sl},$$

where L_m is the latent heat of fusion. Superheating has been shown to have thermal effects on the order of several percent for some laser processing applications, however for the nanosecond timescales which which are our main focus it is considered negligible. Most important for high energy applications (such as ablation) is the possiblity of non-equlibrium processes, such as phase explosion. Such modeling is part of the current proposal. It is a straightforward task to verify the consistency of this assumption. Energy conservation at the liquid/vapor interface requires

$$k_l \frac{\partial T_l}{\partial z} = \rho_l L_v \frac{d}{dt} a_{lv},$$

and the kinetics of evaporation mean that

$$\dot{a}_{lv} = \frac{d}{dt} a_{lv} = v_* e^{-\Delta h / k T_{lv}},$$

where Δh is enthalpy of vaporization (per molecule), v_* is approximately equal to the speed of sound in the material, and T_{lv} is the temperature at the interface. A result of these relations is the fact that T_{lv} can be much larger than T_v, the normal boiling temperature. This temperature also depends on the vapor saturation pressure. The laser-induced heat flux is given by

$$q = (1 - R(T)) e^{-\int_0^z \alpha(T(z'))\, dz'} I(x, y, t),$$

where R is the reflectance, which depends on the photon frequency as well as on the temperature and phase of the material, α is the linear absorbtion coefficient (which also depends on photon frequency and temperature and phase of the material), I is the intensity of light radiation incident on the surface, and z is the distance into the condensed material, normal to the surface. The heating rate density source term is thus, for constant absorption coefficient,

$$Q = (1 - R) \alpha e^{-\alpha z} I(x, y, t).$$

The laser spot is not symmetric and generally a non-trivial function of the tangential variables, x and y. Although the spatial profile of the excimer-type laser illumination spot is usually taken to be roughly rectangular, it varies with time and, particularly,

between shots, in unpredictable ways. The fact is, is it very difficult to measure irradiance at all, let alone in real time. The laser pulse intensity will be assumed to have the characteristic excimer form:

$$I(t) = I_0(\frac{t}{\tau_p})^\mu e^{-t/\tau_p},$$

rather than the Gaussian pulse that is sometimes used (and characteristic of the older generation of lasers). The relation that τ_p, which we will call "pulse length," has to the full-width half-maximum (FWHM) of pulselength is

$$\tau_p/\tau_F \approx 1.2.$$

There are several approaches to the scaling of the problem. If we take as characteristic time scale for the problem, the pulselength τ_p, and from this form the diffusion length, $l_D = \sqrt{D\tau_p}$, which we take to be the characteristic length scale. The diffusivity, D, is defined to be

$$D = \frac{k_s(T_0)}{c_s(T_0)\rho_s}. \tag{4}$$

If material parameters are assumed to be independent of temperature within each phase, then the equations become:

$$\frac{\partial\theta_i}{\partial\tau} = \frac{\partial^2\theta_i}{\partial\zeta^2} + \Gamma P(\zeta,\tau), \quad i = l, s, \tag{5}$$

where

$$P(\zeta,\tau) = e^{-(\alpha l_D\zeta - a_{lv})}\tau^\mu e^{-\tau}. \tag{6}$$

The dimensionless parameter,

$$\Gamma = \frac{\alpha(1-R(T_m))I_0\tau_p}{c\rho(T_v - T_0)},$$

appears multiplying the source (6). From the form of the equation (5), it follows that the dimensionless number, $\Gamma/\alpha l_D$ is a measure of the ratio of absorbed light energy density to energy density needed to reach the vaporization temperature. Numerical computations bear out the intuition that Γ is indicative of maximum temperature rise, while the dimensionless group $\Gamma/\alpha l_D$ gives a lowest-order prediction of the overall phase change.

The boundary condition (3) becomes

$$\theta \to 0, \quad \zeta \to \infty.$$

A purely thermal condition at the melt interface is

$$\frac{\partial \theta_s}{\partial \zeta} - \beta \frac{\partial \theta_l}{\partial \zeta} = \eta_m \frac{da}{d\tau}$$

where $\beta = k_s/k_l$ is the ratio of the conductivities at the melt temperature, and η_m is a dimensionless constant characterizing the relative size of the enthalpy of fusion compared to the rest of the energy required to reach the boiling temperature (this number, for constant parameter values, is the reciprocal of the Stefan number). Values of β are typically $\approx 2.25 - 2.5$ for metals, ≈ 1 for ceramics.

The enthalpy method has been used for computations because it can easily incorporate the nonlinearities due to the temperature dependencies of the material parameters, and, since we are mainly concerned with the approximate size and evolution of the melt region, we don't have to worry about the usual difficulties with front-tracking. The enthalpy, or heat content per unit volume, is given by

$$H = \int_0^T \rho c(T') + \rho L_m \delta(T' - T_m)\, dT',$$

where the specific heat follows an empirical law,

$$c(T) = a + bT + cT^2 + dT^3 + eT^{-2},$$

where the coefficients are tabulated in various references or else matched to data tables or graphs from other sources. The temperature dependency of the thermal conductivity is taken care of using the Kirchoff transformation,

$$W = \int_0^T k(s)\, ds.$$

The nonlinear function, $k(T)$, is much harder to match to a general formula in integral powers of the temperature. A weak formulation of the model is then considered using the variable H and W by using an integral operator form of the heat conservation law. This results in a toughening of the the usual stability condition for the explicit method, and in practice, the time-step is necessarily much smaller than order of square of the space interval.

Figure 2 portrays the results of a calculation using material parameters typical of a "black" oxide, with optical properties between those of a semi-transparent oxides and metals. A small absorption coefficient and low thermal conductivity combine to ensure that the material "sees" a practically uniform body heating. Physically this should correspond to the establishment of a "mushy" region. As is seen in Figure 3, the rise to maximum temperature (just above the melting temperature) is fast. The computed

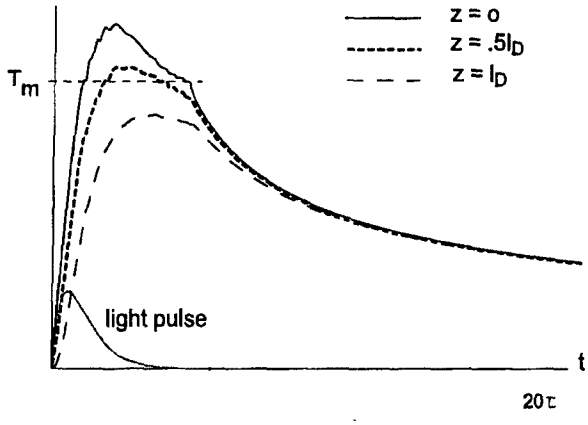

Figure 1:

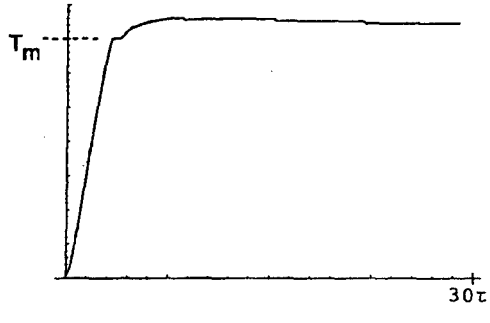

Figure 2:

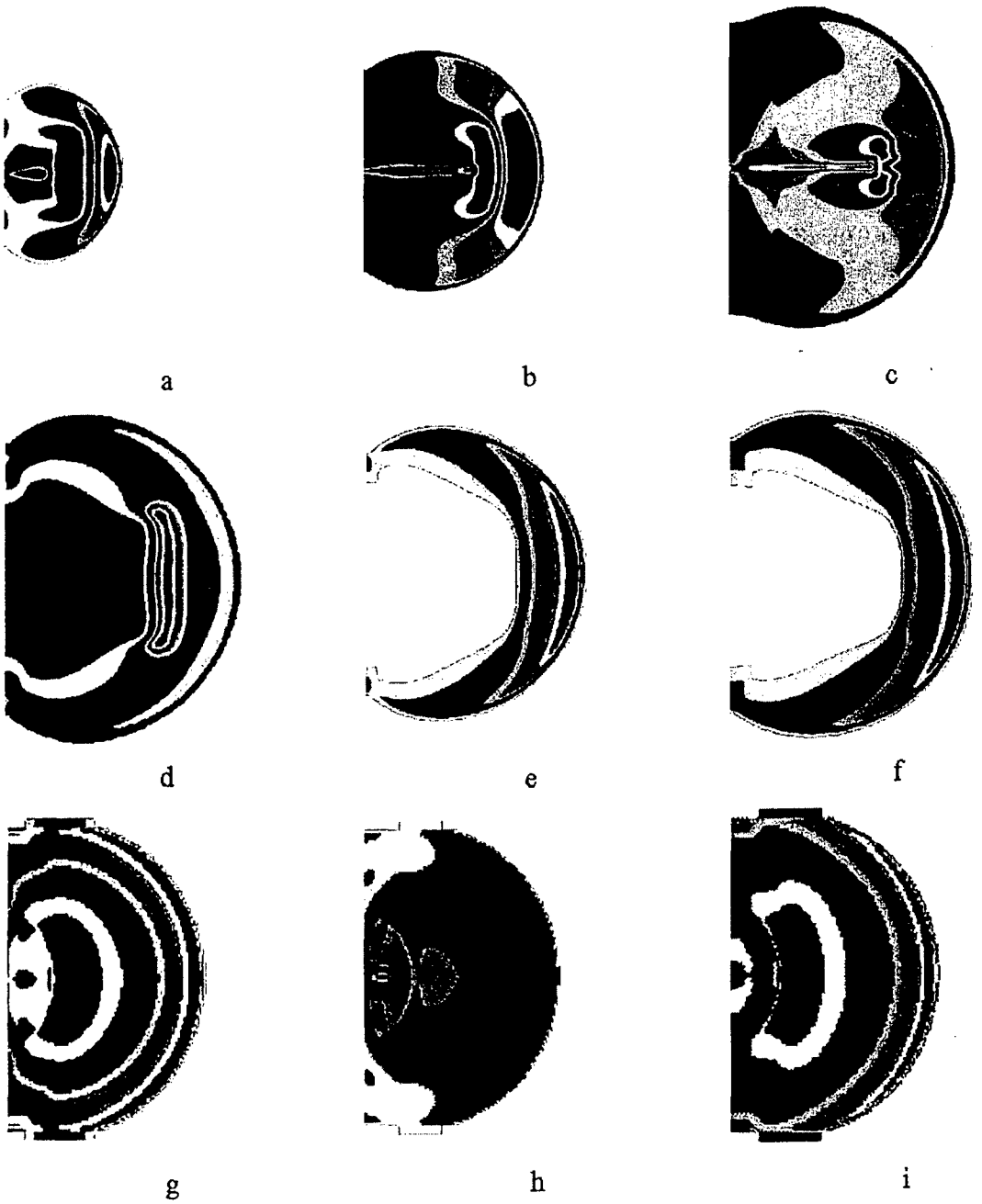

Figure 3:

"mushy" region is clearly visible and lasts several pulselengths; however, when kinetics of nucleation and interface formation are taken into account, along with the minimal temperature rise over the melting temperature, one expects the physical "mushy" region to be more considerable. The time scale is about 30 pulse lengths (close to 1 μs).

In nanosecond pulses of intensity $> 10^8$ W cm^{-2}, energy is transferred to the solid/liquid at such high heating rate that there is a critical or supercritical transition through a metastable phase of solid/liquid/gas. In this regime, the material is far from equilibrium, as, thermodynamically it can be thought of as in a state near the spinodal line where volume fluctuations are high. This means that the material undergoes homogeneous nucleation of vapor regions inside the condensed phase rather than usual boiling. The energy may be released in a shock wave of the multi-phase condensed material. The amount of ablated material depends linearly on the fluence of the laser beam, as long as the intensity is not too high or too low. The ablated material is at extremely high temperatures ($\sim 10^4 - 10^5$K) and thus ionized; the degree of ionization varies according to circumstances, and has been measured as being much higher than predicted by equilibrium considerations (Saha equation). Besides the thermal ionization of the plume, there are other pathways, including photo-ionization and multiphoton absorption. The ionized cloud erupting from the surface can absorb energy from the laser beam. Thus the incipient plume is further heated by this absorption. It is expected that the dominant means of photon absorption in this gas is by three-body interaction involving two electrons and a neutral atom; the degree of ionization of the plume has never been conclusively established by experiment and is presumably very sensitive to control parameters. If the ablation is done into vacuum, the expansion is rapid enough that the bulk of the plume is transparent to the laser beam, and the absorption region is at the gas/condensed interface. This layer is very small relative to the size of the expanding plume and can be considered to be held at a single temperature, since the relaxation here is much faster than the accelerating plume. Expansion into a vacuum proceeds according to free flight where the thermalization of particles never takes place. For near-vacuum depositions, the flight of the plume can be expected to be a Knudsen flow where collisions slowly establish local thermodynamic equilibrium. Film depositions are usually done in an oxidant ambient of about $50 - 300$ mTorr. In this atmosphere, the ablation material is an accelerating jet into the ambient and a compressive shock is formed. This forms the supersonic plume. A one-dimensional model has been constructed using the assumption of equlibrium phase kinetics and the use of the Knudsen-Layer as a hydrodynamic discontinuity. For this model, the resulting hydrodynamics depends on the single parameter of the surface temperature, which, however, depends on control parameters in a complicated way.

Regarding the hydrodynamics and chemistry of the plume, we developed both analytical and computational models. We were particularly interested in resolving questions

that arose during analysis of experimental data, particularly time-of-flight measurements from emission spectroscopy. In the plume itself the general conservation laws are valid. That is, for general regions, V, and times, t_1, t_2, a system of integral equations,

$$\int_V \mathbf{G}(\mathbf{r}, t_2) - \mathbf{G}(\mathbf{r}, t_1)\, d\mathbf{r} = \int_{\partial V} \mathbf{F} \cdot d\mathbf{S},$$

holds, where $\mathbf{G}$ is a vector of conserved quantities and $\mathbf{F}$ is a tensor of fluxes. In order for this to reduce to a differential model, we need to identify some small size V so that thermal equilibrium (among any components lumped together) is *instantaneously* established on this scale (as far as the model is concerned). Here, we identify such a dimension with the mean free path based on densities encountered in the deposition chamber. The pulsed laser ablation plume is made up of M components, of varying mass. Let n_i denote the (particle) concentration of the *ith* species, and m_i the (particle) mass of the *ith* species, then define the peculiar velocities in the following way: each particle of the *ith* species has a velocity

$$\mathbf{v}_i = \mathbf{v} + \mathbf{V}_i$$

where $\mathbf{v}$ is the bulk flow velocity and $\mathbf{V}_i$ is the peculiar velocity of the *ith* species. Note that in the particle phase space, each particle takes on the local momentum:

$$m_i \mathbf{v}_i = \mathbf{p}.$$

After Boltzmann averaging and mass-averaging over the species, we get a local flow velocity defined by

$$\rho \mathbf{v} = < \sum \rho_i \mathbf{v}_i >_p = \sum \rho_i < \mathbf{v}_i >_p,$$

where $< \ >_p$ denotes the Boltzmann averaging over momentum space. The peculiar velocity has the average,

$$< \mathbf{v}_i >_p = \mathbf{V}_i^d,$$

which we call the molecular diffusion velocity, so that

$$\mathbf{v}_i = \mathbf{v} + \mathbf{V}_i^d + \mathbf{V}_i',$$

where $\mathbf{V}_i'$ is the "chaotic motion" of the *ith* species. This allows us to define a temperature for the *ith* species,

$$T_i = \frac{m_i}{2c_{vi}} < |\mathbf{V}_i'|^2 > .$$

By averaging over scales smaller than the characteristic length scale identified above, we can derive the conservation laws valid on larger scales. The species mass conservation takes the form

$$\frac{\partial}{\partial t} n_i + \nabla \cdot (n_i(\mathbf{v} + \mathbf{V}_i^d)) = g_i, \quad 1 = 1, \ldots, M,$$

where g_i is the species production or decomposition due to chemical reactions. This equation could also be written in terms of the mass densities, $\rho_i = n_i m_i$, or the mass-fractions, ρ_i/ρ. Multiplying by m_i and summing over i, and using

$$\sum m_i n_i < \mathbf{V}_i^d >= 0,$$

we get the bulk mass conservation equation,

$$\frac{\partial}{\partial t}\rho + \nabla \cdot (\rho \mathbf{v}) = 0.$$

The equation of motion for the mixture,

$$\rho \frac{\partial}{\partial t}\mathbf{v} + \rho \mathbf{v} \cdot \nabla \mathbf{v} + \nabla \cdot \mathcal{P} = 0,$$

is written in terms of a total pressure tensor. If we assume that $< \mathbf{V}_i >^2 \ll < \mathbf{V}_i'^2 >$, which will be valid except in "collisionless" flow, then we can derive equations for the temperatures. The total pressure tensor is written

$$\mathcal{P} = \sum \mathcal{P}_i,$$

where the pressure for each component is that of an ideal gas,

$$p_i = \rho_i \frac{R}{m_i} T_i.$$

The overall mixture will then satisfy an ideal gas law,

$$p = nRT,$$

if we define a (mixture) temperature as

$$T = \frac{1}{n} \sum n_i T_i,$$

where $n = \sum n_i$. (This was the whole point of defining things this way. We will deal with an inviscid fluid, so there is no ambiguity about the meaning of pressure.)

The specific enthalpy,

$$h = \int^T c_p \, dT + \rho^{-1} \sum \rho_i \, \Delta_f H_i,$$

is conserved. Here, $\Delta_f H_i$ is the heat of formation of the ith species, and T is the total mixture temperature as defined above. In this way, the energy source (sink) of

an exothermic (endothermic) reaction is taken into account. At the rapid flow accelerations in the plume, the entropy variation is small and therefore the reaction term is immediately converted into a change in temperature.

It is easy to estimate characteristic scales and relative importance of transport mechanisms, based on a one-dimensional model of the preparation of the blow up to the nether edge of the Knudsen Layer. A mean free time between collisions is estimated as $10 - 20$ ns, while the characteristic time for total (mean) momentum to be transferred across features of the plume by collisions is about 100 times longer. This is the main reason that we consider an inviscid flow. However, because of the large temperature gradients that are set up by the shock heating in the supersonic plume, and the interaction with chemical reactions, we must allow for thermal conduction and species diffusion.

In short, the inviscid hydrodynamic equations with heat and mass diffusion and heat production by reactions, comprise our basic model according to the approximation above. We carry out a preliminary one-dimensional inviscid calculation and then a two-dimensional transport calculation with the chemistry accounted for in a simplified scheme which is explained in what follows, as we focus on the chemistry of the plume (Figure 2). Metal vapor, atomic and molecular oxygen (and/or other oxidizers) and any relevant metal-oxide are the components of the plume. We will make the case that the primary reaction in our scheme is the termolecular oxidation reaction. In the nascent plume, one expects to see bimolecular exhange reactions, governed by arbitrary high kinetic energy collisions, such as

$$\mathrm{M} + \mathrm{O}_2 \longrightarrow \mathrm{MO} + \mathrm{O}$$

These reactions have high activation energies and should constitute the main scheme in the Knudsen layer and at its edge. After a period that is on the order of $10 - 100$ ns, the metallic vapor has been excited and starts recombination and de-excitation due to collisions and photon release. The characteristic times of the bimolecular reactions show the scaling

$$\tau_{bimol} \propto \rho_k e^{-E_a/kT}.$$

These "endothermic" reactions establish strong localized temperature gradients. On the time scales of the fully formed plumes simulated here, termolecular reactions, such as the oxidation

$$2\mathrm{M} + \mathrm{O}_2 \longrightarrow 2\mathrm{MO},$$

or the recombination reaction

$$\mathrm{M} + \mathrm{O} + \mathrm{O} \longrightarrow \mathrm{O}_2 + \mathrm{M},$$

will predominate. These are heat producing reactions that are self sustaining on relatively long time scales, even as the plume is cooling due to expansion. For these reactions, the characteristic time scale is

$$\tau_{termol} \propto \rho_M^2,$$

proportional to the density of metal atoms, and we expect that this will lead to equilibrium densities. In this way, we are led, in short order, through an initial oxide formation via the endothermic bimolecular reactions in the nascent plume, cooling by expansion as the plume loses its one-dimensional character, balanced by the heat-producing reactions which are sustained through until equilibrium is achieved.

Figure 4 shows the results of a two-dimensional simulation of the plume equations carried out by use of a finite-volume method. The top row shows the temperature distributions at 2 different times, (a) 0.5μs, (b) 1.0μs, (c) 1.5μs, for a case of medium-high energy input. The second row shows the density and pressure distributions for the same case. The third row shows the density, temperature, and pressure distributions for a case for smaller energy input at a time of 2μs. The approximate size of each picture is a centimeter. Thus, the lower energy jet has a less-pronounced shock, and more spherically symmetric temperature distribution.

The difference between the computed plumes without substrate heating (Figures 4 and 5) differ dramatically from the computed plumes in the presence of a temperature gradient (Figures 6, 7, 8), conforming to the difference that one observes in the actual plume.

The pictures of a plume, either in vacuum, or in ambient without substrate heating show the usual rounded cosine shape, but when substrate heating is present strong vorticity is generated at the 'wings' of the plume, leading to recirculating flow, greater mixing, and thermalization in those regions, but allowing a more focussed quasi-one-dimensional jet to be produced along the flow axis as the plume nears the substrate heater. One of the prominent features observed in the simulations are relatively large scale vortices at the oblique wings of the plume. Recirculating flow and strong mixing occur there giving rise to collisional processes that result in a strong emission sometimes showing a double peak in the density time-of-flight. The sense of the vortices is what we will refer to as *expected orientation.* A comprehensive collection of simulation results, including animations, can be found on the author's web site.

The expression for the vorticity, $\boldsymbol{\omega} = \text{curl}\,\mathbf{u}$, is, in these coordinates,

$$\boldsymbol{\omega} = \left(\frac{\partial w}{\partial s_2} - \frac{1}{h_2}\frac{\partial (h_2 v)}{\partial n}\right)\mathbf{t}_1 + \left(\frac{1}{h_1}\frac{\partial (h_1 u)}{\partial n} - \frac{\partial w}{\partial s_1}\right)\mathbf{t}_2 + \left(\frac{1}{h_2}\frac{\partial (h_2 v)}{\partial s_1} - \frac{1}{h_1}\frac{\partial (h_1 u)}{\partial s_2}\right)\mathbf{n},$$

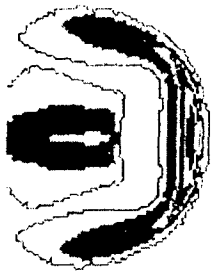

Figure 4: Computed shock wave of an ablation plume. Temperature contours are shown.

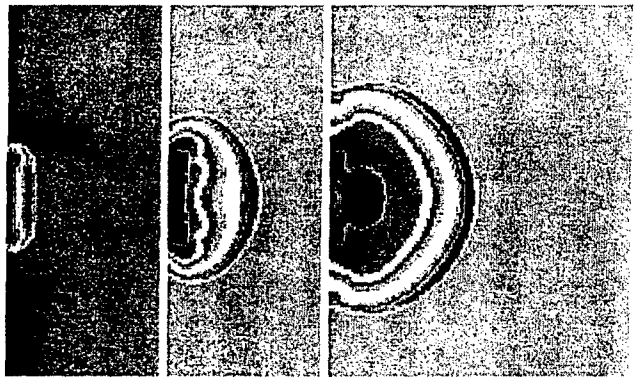

Figure 5: Computed shock wave of an ablation plume. As in Figure 4, temperature contours are shown. The operating conditions are different than in that case.

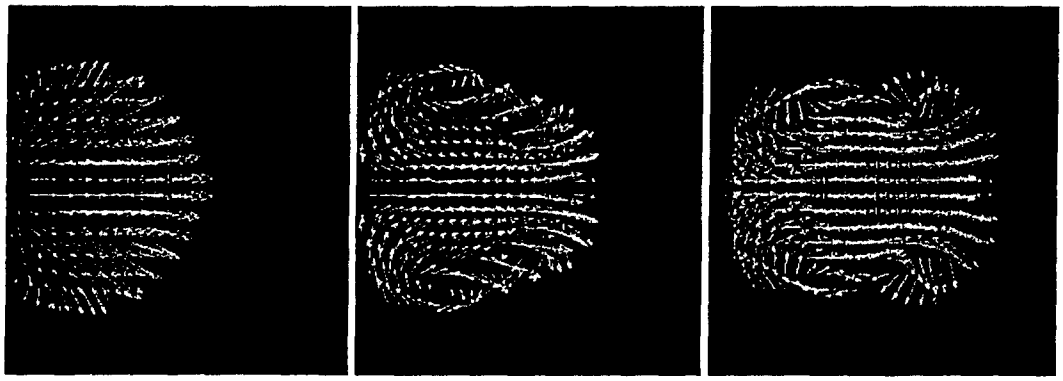

Figure 6: Temperature distribution (color) and velocity vectors at three successive snapshots of a plume in an applied temperature gradient, taken about 1 μs apart. It is apparent that in this case a strong recirculating flow is developing.

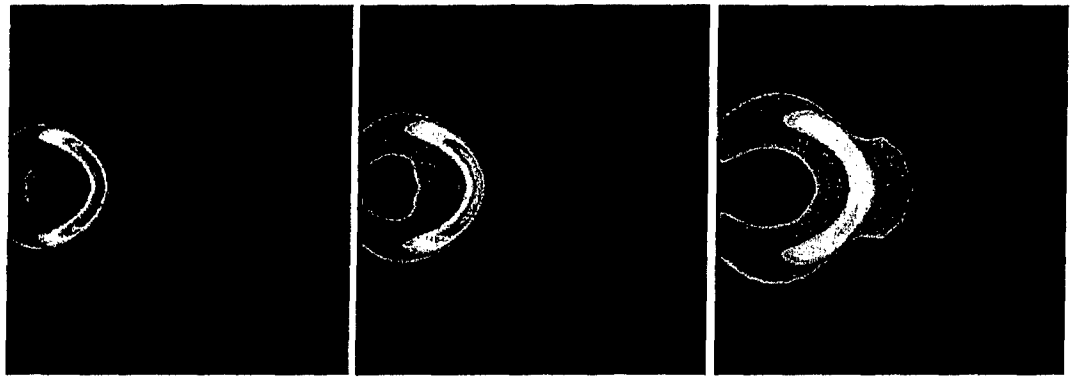

Figure 7: Contours of the temperature distribution in the devloping plume, for a set of operating conditions similar to Figure 5 except for the presence of a temperature gradient.

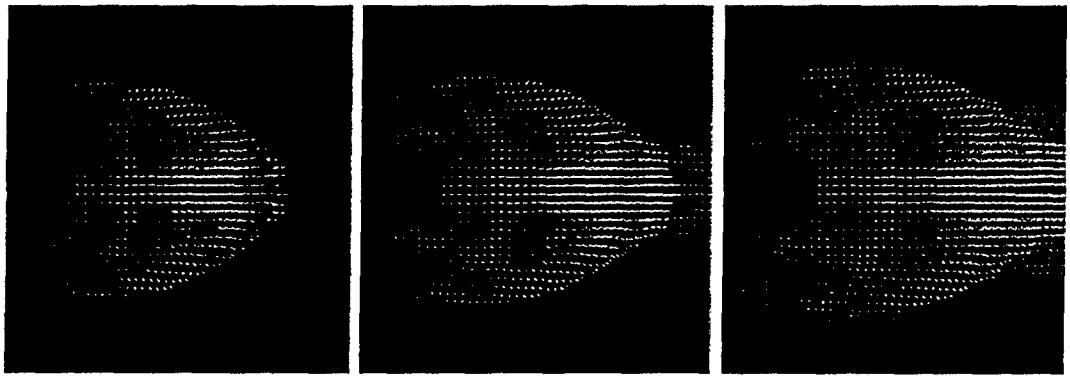

Figure 8: Enthalpy (color) and velocity vectors in yet another case. This case corresponds to a greater energy deposition.

$$[\![\boldsymbol{\omega}_{tan}]\!] = \mathbf{n} \times \left([\![\frac{1}{\rho}]\!] \nabla_{tan}(m_s) + [\![\rho]\!] (\frac{V_n}{m_s})(\mathbf{S}(\mathbf{u}_{tan} - \mathbf{V}_{tan}) - \dot{\mathbf{n}}) \right), \tag{17}$$

where we have only included terms that are consistent with the assumption that the shock moves into quiescent gas.

It is the first term in the above expression that involves the thermal gradient in the quiescent gas. The other term, involving the jump in density, is made up of two terms, the first is related to the curvature of the shock front, and the second involves the local rotation of the shock. In order to estimate the relative importance of these terms an analytic expression for the thermal field in the quiescent gas will be used. We can approximate the heated substrate by a flat disk, radius a, held at a fixed temperature, T_s, and, given the geometry, sizes, and materials involved, the temperature at infinity can be taken to be room temperature, T_R. Using the nondimensionalization, $\theta = \frac{T - T_R}{T_R}$, and

$$\frac{\rho}{\rho_{ref}} = \frac{1}{1+\theta} = \frac{1}{1 + \theta_s \text{arccot}(\frac{z}{a\cos\theta})}, \tag{18}$$

where θ_s is a nondimensional parameter of order approximately unity when the substrate temperature is in the range

$$T_R < T_s < 4T_R,$$

which is essentially the experimentally considered range. It is reasonable to assume that the density behind the shock is constant. From the functional form of (18) it is seen that there are essentially two regimes: for distances from the target on the order of a, the term $[\![\frac{1}{\rho}]\!]$ is at least an order bigger than $[\![\rho]\!]$. Let us examine this expression locally. Assume a planar shock, oriented parallel to the $\mathbf{i}$ axis where the $\mathbf{k}$ axis is perpendicular to the substrate pointing at the target, with $\mathbf{V} = -V(t)\mathbf{k}$, and $\mathbf{n} = -\cos\theta\mathbf{k} + \sin\theta\mathbf{j} = \sin\psi\mathbf{k} + \cos\psi\mathbf{j}$. (Here, ψ is the complement of θ.) This θ is a local parameter, but can be associated with the global variable, θ, for a shock that is approximately spherical. (By choosing this form for the tangent plane, we are assuming an axi-symmetric plume.) In the same way, we will use the variable, z, which can be replaced by $\frac{z}{a\cos\theta}$ in a global treatment. The mass flux is $m_s = \rho \sin\psi V$, and

$$\nabla_{tan}(m) = -\cos\psi \sin\psi V \frac{\partial \rho}{\partial z}. \tag{19}$$

Since $[\![\frac{1}{\rho}]\!]$ is negative, the vorticity produced is of the *expected orientation.* Furthermore, in the early regime, before the plume decelerates and while that factor is large, the term (19) is small along the longitudinal axis of the plume and only is significant off-axis. Now let us examine the rotation term, using the same local plane. Here, $\dot{\mathbf{n}} = \boldsymbol{\Omega} \times \mathbf{n}$. First, consider the rotation towards or away from the substrate, i.e., $\boldsymbol{\Omega} = \omega\mathbf{i}$, with $\omega < 0$

or $\omega > 0$, respectively. This gives rise to a transverse vorticity production term,

$$-\omega(\frac{V_n}{m})[\![\rho]\!]\mathbf{i}.$$

Furthermore, this term is opposite signed to that which would be produced due to the curvature. An arbitrary rotation can produce streamwise vorticity as well; let $\mathbf{\Omega} = \omega_x\mathbf{i} + \omega_y\mathbf{j} + \omega_z\mathbf{k}$, then the corresponding vorticity production term is

$$[\![\rho]\!](\frac{V_n}{m})(-\omega_x\mathbf{i} + (\omega_z\cos\psi - \omega_y\sin\psi)\mathbf{X}),$$

where $\mathbf{X}$ is a unit vector along the tangent plane, perpendicular to $\mathbf{i}$. Note that streamwise vorticity production can be zero even in the presence of rotation. This generation of vorticity is especially important when one takes into account the interaction of relaxation and reaction mechanisms. This is the focus of ongoing research.

Concerning the theory of magnetocaloric effect in magnetoelasticity, we can derive interesting results under the condition of weak, but non-negligeable interaction. This weak collective excitation scheme was then carried over by analogy to the excitations of the flux-line lattice in type-II superconductors (HTSC) in the mixed state. It may seem at first that this is a completely different situation, but, as long as the same statistics hold (this is regime of linear excitations), the situations will be similar when the energies behave similarly.

The history of investigations into the magnetocaloric effect has shown that sharp changes in the isentropic curves, are associated with phase changes. These investigations usually rigorously focus on the entropy of the magnetic system and do not take explicit account of the vibrations of the material structure, except to accord it the status of heat sink. In a magnetic system, for example, there is a coupling between the excitations of the magnetic systems (magnons) and the vibrations of the crystal lattice (phonons) and the condition becomes

$$S_{mag} + S_{phon} = \text{constant}.$$

If the crystal lattice is simply a heat sink then the effect of the phonons is, broadly put, to weaken the magnetocaloric effect, but does not qualitatively affect the calculation, in particular, the sign of the effect. The criteria governing the validity of this assumption can be made explicit by reference to the relevant relaxation times of the various modes of dissipation.

A Hamiltonian was used to account for the magnetoelastic interactions in a uniaxial ferromagnetic crystal,

$$H = H^{magnetic} + H^{magnetoelastic} + H^{elastic},$$

where

$$H^{magnetic} = aM^2 + A(\nabla \mathbf{M})^2 - \beta(\mathbf{M}\cdot\hat{\mathbf{z}})^2 - \mathbf{M}\cdot\mathbf{H},$$

where $\mathbf{M}$ is the (macroscopic) magnetic moment density, $\mathbf{H}$ is the external magnetic field, a, A are exhange coefficients, β is the anisotropy coefficient (the easy axis of magnetization is the z-direction). The crystal is assumed to be isotropic (cubic), and the energy stored in the elastic deformation is

$$H^{elastic} = 2\lambda u_{l,l}^2 + \mu(u_{i,k} + u_{k,i})^2,$$

where $\mathbf{u} = (u_x, u_y, u_z)$ is the material deformation vector,

$$u_{k,i} = \frac{\partial u_k}{\partial x_i},$$

and λ, μ are the isotropic elastic moduli. The interaction energy is given by

$$H^{magnetoelastic} = g\mathbf{M}\cdot(\mathbf{M}\cdot\nabla)\mathbf{u}.$$

The Hamiltonian was diagonalized by a method of second quantization, leading to a 8^{th}-order secular equation for the energies of the collective excitations of the combined magnetoelastic system. Special solutions can be found corresponding to a (quasi-) magnon branch and three (quasi-) phonon branches. In other words, we continue the branches that start at $g = 0$, corresponding to spin waves and to sound waves propagating along symmetry axes having two degenerate transverse waves. This spectrum is valid under the assumption of weak interaction

$$(\Delta l/\beta \ll 1).$$

Then, the results of the calculation are that

The quasimagnon spectrum is

$$\Omega_m^2 = \epsilon_k^2 + c_l\varphi(k_x^2 + k_z^2).$$

The quasiphonon spectrum is

$$\Omega_3 = c_l k,$$

$$\begin{aligned}\Omega_{1,2} &= \frac{1}{2}[c_t^2 + c_l^2 - \varphi c_t^2(\kappa_x^2 + \kappa_z^2)] \\ &\pm[\frac{1}{4}[c_t^2 + c_l^2 - \varphi c_t^2(\kappa_x^2 + \kappa_z^2)]^2 - c_t^2 c_l^2[1 - \varphi(\kappa_x^2 + \kappa_z^2) + 4\varphi c_t^2(c_t^2 - c_l^2)(\kappa_x^2\kappa_z^2)]]^{1/2},\end{aligned}$$

where

$$\varphi = \frac{\Delta l}{\Delta l + \Delta h}(\kappa_x^2 + \kappa_z^2),$$

is a kind of order parameter. The c_t, c_l are the usual transverse and longitudinal sound-speeds. It is seen that the branch corresponding to Ω_2 has the peculiarity of disappearing at the approach of the phase transition,

$$(\Delta h \ll 1),$$

in the directions of the magnetic field and of the easy axis. It is the nature of boson statistics that as a quasiphonon branch goes to zero in the neighborhood of the critical field, the total energy stored in the corresponding collective excitations,

$$E = \sum \omega_k n_k,$$

increases. In other words, one is not penalized by transferring bosons to this mode. This means that in the equilbrium corresponding to the increased field, energy will be transferred to quasimagnons from quasiphonons. This will mean a lowering of the temperature, thus one would expect a negative magnetocaloric effect in the neighborhood of the phase transition. A similar effect wherein occurs change of polarization of sound waves has been observed in experiments with AC magnetic pulses. It would appear that a simplified model is called for that can be integrated over the whole Brilluoin zone in order to compute the entropy but still reproduces the behavior of this spectrum along the symmetry axes. In the simplest model of this sort the spectrum could be written in the form:

magnon frequencies

$$\Sigma_k^2 = [\alpha k^2 + n_3][n_3 \cos^2\theta + \alpha k^2],$$

phonon frequencies

$$\omega_{1,2}^2 = k^2\{n_0 \pm \sqrt{n_0^2 - n_1 \cos^2\theta \frac{k_x}{k}}\}, \tag{20}$$

$$\omega_3^2 = n_2 k^2, \tag{21}$$

where

$$\cos^2\theta \propto |1 - h| = |\frac{H - H_A}{H_A}|.$$

The isentropic curves for this system show a very strong negative magnetocaloric effect at a field at a finite distance below the critical field.

According to the Ginzburg-Landau-Abrikosov theory, the flux line lattice of vortices in a type-II superconductor has a "magnetoelastic" interaction built into it. If we assume a linear elastic description of the flux line lattice, then there are independent modes of oscillation, shear, compression, and tilt waves; all of these carry the magnetic interaction with them. For the high-temperature superconductors with their large values of the Ginzburg-Landau parameter, κ, we should expect a large negative magnetocaloric effect. For small values of the flux, the elastic energy is proportional to the square of the flux, so we should expect a positive magnetocaloric effect, as for the ferromagnet, only for vanishing fields. Both the flux penetration depth, λ, and the coherence length, ξ, diverge as $\approx (1 - B/B_{c2})^{-1/2}$ as the flux approaches the upper critical field, B_{c2}. This means a vanishing of the elastic exitation energy of the flux line lattice as the upper critical field is approached, leading us to consider approaching this situation in a way analogous to the magnon-phonon interaction. For a uniaxial flux line lattice where the flux is always perpendicular to the ab-plane, and we ignore elastic interactions with pinning caused by material inhomogeneities, the flux-line lattice modes have the elastic energy matrix elements

$$\phi_{ij} = (c_{11}(b,k) - c_{66}(b))k_i k_j + \delta_{ij}(c_{66}(b)(k_x^2 + k_y^2) + c_{44}(k,b)k_z^2)$$

The computed isentropic curves for shear excitations show a monotone negative magnetocaloric effect. In the isentropic curves for excitations corresponding to isotropic compression waves there is an interesting change of sign of the magnetocaloric effect at a low value of the magnetic field. Previously, such behavior had been associated with antiferrimagnetic systems. We have identified a possible test material, a nanocrystalline superparamagnetic material. Besides being designed to match a certain model of magnetoelasticity, this material system is an example of a mesoscopic system with significant interactions in the nanometer-micron range. The manipulation and process control of the spatial and temporal structure of matter over mesoscopic distance scales, especially near phase transitions, has been identified as important to the long-range war-fighting capabilites of the Air Force.

Personnel Supported

Besides the PI, no personnel were directly supported on this grant. However, the PI has collaborated with colleagues at Wright State and other Institutions, has been aided by students who are supported through other grants, and has hired hourly workers.

Publications

Technical Reports

1. Annual Scientific Report February, 2000
2. Annual Scientific Report November, 2000
3. Annual Scientific Report September, 2001

Scientific Publications

1. Energy flow in the laser treatment of materials (submitted summer 2000 to Applied Mathematical Modelling, currently being revised)
2. Reacting flow in a pulsed-laser ablation plume (submitted March 2001 to Applied Mathematical Modelling)
3. Flux flow relaxation and the shape of magnetic hysteresis loops in type-II superconductors (submitted to Physica C)
4. The Pulsed-Laser-Ablation plume in a thermal gradient (submitted to Physics of Fluids)
5. Simulation of the pulsed laser ablation plume under a thermal gradient, (with S. Raghuram)
6. The pulsed-laser ablation plume dynamics: characterization and modeling (with R. Biggers), High Power Laser Ablation SPIE 2002
7. Reacting Dynamics of the Laser Ablation Plume (with R. Biggers), AIAA-2003 paper 0678

Collaborative Activities and Interactions

Local Activities

Air Force Research Lab interactions

The main interaction with AFRL involved a collaboration with the experimental PLD group at AFRL/WPAFB. The coordinator of this project is Rand Biggers (MLPS), but involves the participation of the following Branches MLPS (Sensor materials), MLMR (Manufacturing technology) of the Materials Directorate, PRPS of the Power Directorate, as well as contractors from UDRI, WSU, UES, Mound Laser and Photonics, and AFIT. Other people involved in this project are I. Maartense, G. Kozlowski, L. Dosser, D. Dorsey, G. Perram, T.L. Peterson, J. Maguire, A. Jackson, J. Busbee, J. Jones, N. Boss. The PI has also interacted with Air Force personnel interested in picosecond and femtosecond pulsed laser interaction with matter, and with scientists interested in fabricating ferroelectric materials. The PI has interacted on several occasions with scientists from AFRL Air Vehicles Directorate and have generated research proposals. The PI has also interacted with the Human Effectiveness directorate concerning physiological modeling. This collaboration has been successful in attracting funding (B. Foy of the Physics Dept at Wright State is the PI on grants from AFOSR and DAGSI). This research supports the AF lab investigating toxicity, and survivability in toxic environments.

Activities at Wright State University

I have run an Applied Math/Physics/Modeling Seminar. Speakers that were partially supported by this grant were M. Gunzburger of Iowa State (who spoke on numerical methods), S. Shen of NASA/GSFC (who spoke on data mining), and V. Rao of the Swedish Technical Institute (who spoke on non-linear susceptibility in superconductors). Speakers in the seminar from AFRL include J. Maguire, G. Kozlowski, V. Venkayya, C. Pettit, and T. Knox. The PI has also hosted visitors from University of Utah, Iowa State University, Charles University, and New Jersey Institute of Technology.

Out-of-Town Activities

In June 99, I gave an invited talk at the annual meeting of the Canadian Applied and Industrial Math Society. In July 99, I traveled to Eger, Hungary, and spoke at the Summer School on High Temperature Superconductivity [most of expense paid for by host]. In September 99, I traveled to Ames, IA, to discuss superconductivity with M. Gunzburger [most of expense paid for by host]. In October 99 I travel to College Station, Texas, and gave an invited talk at the International Conference on Nonlinear Control Theory [most of expense paid for by host]. In December 99, I traveled to Prague, CR, collaborate with Z. Kalva on the magnetocaloric effect [most of expense paid for by host]. I presented a poster at the American Physical Society March 2000 meeting in Minneapolis. In October 2000, I presented an invited talk at the International Conference on Control in Raleigh, N.C.; in November 2000, I gave a talk at the APS Annual Meeting of the Division of Fluid Dynamics in Washington, D.C.; in March 2001, I presented a poster at the Annual Meeting of American Physical Society in Seattle, WA.; in April 2001, I gave an invited talk at the American Mathematical Society Western Regional Conference in Las Vegas, NV. I presented a poster in March 02 at the Annual Meeting of American Physical Society, Indianapolis, IN; iin April 2002, I gave a talk at the SPIE High Power Laser Ablation, in Taos, NM. I have attended workshops on computational methods in in Detroit, MI; Kent, OH; Columbus, OH; Urbana, IL. I have given presentations at AFOSR Contractors meetings in Stanford (2000, 2001) and Florida (2002).